Electronic Supplementary Material (ESI) for Journal of Materials Chemistry C.

Electronic Supporting Information

Reversible Switching of the Au(111) Work Function by Near Infrared Irradiation with a Bistable SAM Based on a Radical Donor-Acceptor Dyad

Valentin Diez-Cabanes, Andrés Gómez, Manuel Souto, Nerea González-Pato, Jérôme Cornil, Jaume Veciana*, Imma Ratera**

Contents

1. General methods

All reagents and solvents employed for the syntheses and preparation of the SAMs were of high purity grade and were purchased from Sigma-Aldrich Co., Merck, and SDS. Compounds **1** and **2** were synthesized and characterized as previously reported.[1]

2. Working principle of Kelvin Probe Force Microscopy (KPFM)

When the tip and the sample are electrically connected, Fermi level alignment occurs upon electrical contact of the materials, through an electron transfer from the sample into the tip. This transfer induces an offset between the vacuum levels of the two materials, and a contact potential difference $V_{CPD} = \phi_{tip} - \phi_{sample}$. Electrostatic forces F_{el} appear between the two charged surfaces in close proximity from each other. These electrostatic forces are measured and a DC bias (V_{DC}) equal to V_{CPD} is applied to the tip, in order to cancel the electrostatic forces and restore the initial offset between the Fermi levels. By using a calibrated tip with a known work function, the determination of V_{CPD} allows accessing the work function of the sample.

In KPFM, the detection system for the determination of the surface potential is operated dynamically. In order to isolate the electrostatic contribution from the other forces acting between the tip and the sample, a modulated bias ($V_{AC}\sin(\omega_{KPFM}t)$) is applied to the tip, in addition to the static V_{DC}. As the tip is brought in the proximity of the sample, the cantilever therefore experiences an oscillating electrostatic force. Since the tip-sample system can be seen as a capacitor, the electrostatic forces can be expressed as:

$$F_{el} = \frac{1}{2}\frac{\partial C}{\partial z}[(V_{DC} - V_{CPD}) + V_{AC}\sin(\omega_{KPFM}t)]^2 \tag{S1}$$

The development of Eq. S1 leads to three components:

$$F_{el} = F_{el,DC} + F_{el,\omega_{KPFM}} + F_{el,2\omega_{KPFM}} \tag{S2}$$

Where the $F_{el,\omega_{KPFM}}$ component is equal to:

$$F_{el} = \frac{\partial C}{\partial z}(V_{DC} - V_{CPD})V_{AC}\sin(\omega_{KPFM}t) \tag{S3}$$

By isolating and detecting this component, the V_{DC} bias can be adjusted in order to nullify this signal when $V_{DC} = V_{CPD}$.

3. Estimation of the tip-sample distance

The tip vibration is the same before (dark) and after (light) 950 nm irradiation and equal to 21 nm. However, the «electronic» signal acquired by the photodetector is different, as the photodetector is sensible to IR light at 950 nm. The tip is vibrating at its free amplitude modifies while the servo approaches the tip to the surface. As the surface first touches the surface (point A) the amplitude is reduced because the tip cannot vibrate free anymore. Once the tip is indented into the sample, the amplitude of vibration is zero. The difference between point A and point B is the free amplitude of the tip, while we work with a set point which is 80% of this free amplitude. This data provides us the tip-sample distance equal to 16.8 nm.

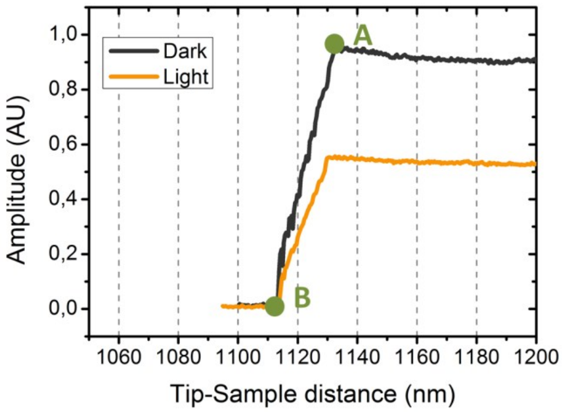

Fig. S1. Vibration Amplitude (AU) vs Tip-Sample distance (nm) after (light) and before (dark) irradiation with 950 nm light.

4. Computational details

As we mentioned in the main text, the methodology used in the MM/MD simulation follows the same procedure as in Ref. S2. The atom types were described at a quantum-chemical level, with atomic charges calculated from the ESP charges[3] obtained at the MP2/cc-pvdz level of theory[4] on the previously optimized geometries, using the Gaussian09 package.[5] In the case of molecule **2**, the Restricted Open-shell (RO) formalism was adopted in order to avoid the problems in Moller-Perturbation Theory related to spin contamination.[6] The three Au layers have been considered as an infinite rigid-body frozen in space to reduce the computational cost. The total replicated unit cell of the SAMs has the following parameters: a=b=93.16Å, c=60Å and γ=60°. The resulting unit cell containing 64 molecules was first optimized at the molecular MM level with the Universal Force Field[7] using the default parameters implemented in the Materials Studio 7.0 package.[8] The atom based summation was used to describe the non-bonded interactions. The optimized unit cell was then used as the starting point for a quenched MM/MD run carried out under NVT conditions (constant number of particles, volume, and temperature) and Nose thermostat. The quenched run was carried for 100-ps and frames were saved every fs. The geometries were extracted every 1000 steps and minimized (i.e., quenched) at the MM level, resulting in a total of 100 geometries.

5. Supporting Figures and Tables

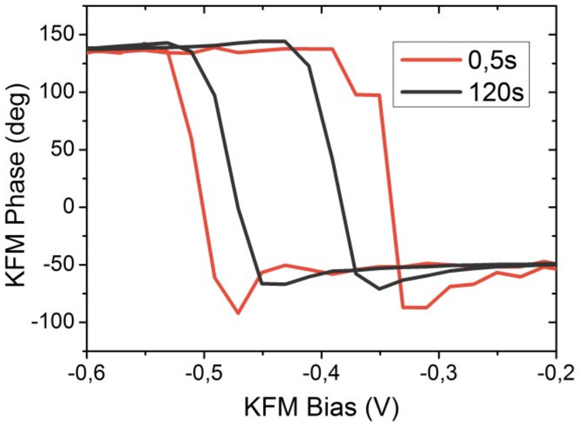

Fig. S2. KFM Phase vs Bias hysteresis cycle evolution with the bias cycle time *t* for **S2**.

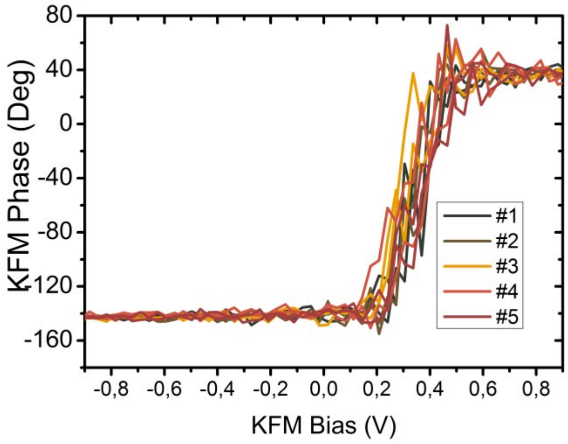

Fig. S3. Hysteresis curves after (light) and before (dark) irradiation with 950 nm light for the Au(111) substrate. Each of the lines represents a separate curve performed different randomized spots of the sample. Note that in this case the Au substrate has been exposed as the same cleaning and preparation processes as the conditions used during the SAMs formation.

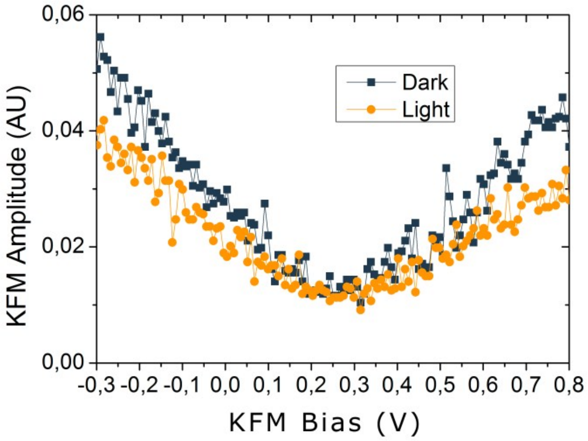

Fig. S4. Surface potential curves after (light) and before (dark) irradiation with 950nm light for the Au(111) substrate. Note that in this case the Au substrate has been exposed as the same cleaning and preparation processes as the conditions used during the SAMs formation.

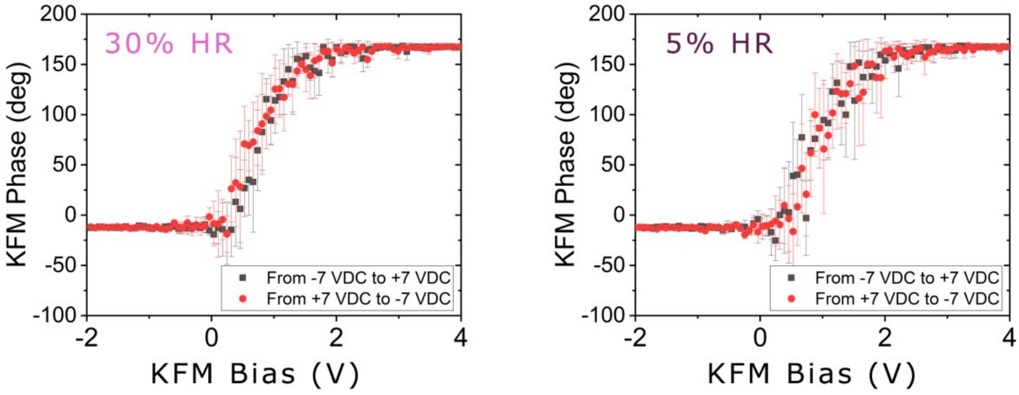

Figure S5: KFM Phase (deg) vs KFM bias (V) for our test sample composed of a gold layer over glass substrate with 30% of RH (left) and 5% of RH (right). The curves are performed with similar conditions as the zwitterionic sample. Our data shows no hysteretic behavior within high humidity environments which should be expected for an electrochemical (humidity) related phenomena. Note that in this case the Au substrate has been exposed as the same cleaning and preparation processes as the conditions used during the SAMs formation.

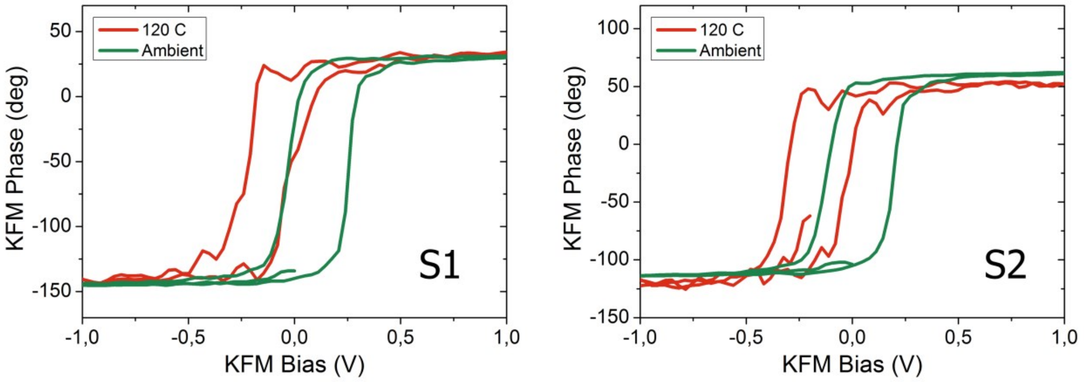

Fig. S6. KFM Phase vs Applied Bias hysteresis curves for room temperature (green), and 120ºC (red); in **S1** (left) and **S2** (right).

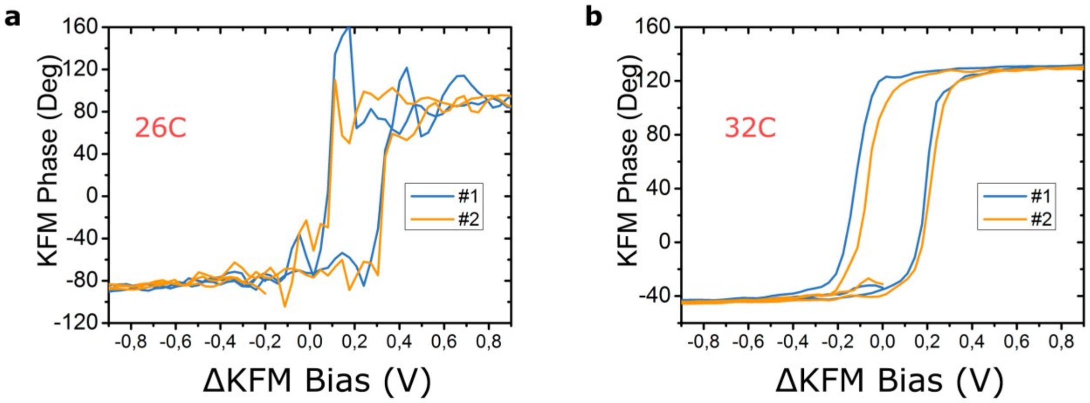

Fig. S7. KFM Phase (deg) vs ΔKFM Bias (V) for the case of the sample **S2**. The initial state of the sample obtained at 26 ºC, **a**, is recovered after the full heating and cooling cycle is finished at 32 ºC, **b**. We observe that the system recovers its original behaviour while returning at the initial room temperature.

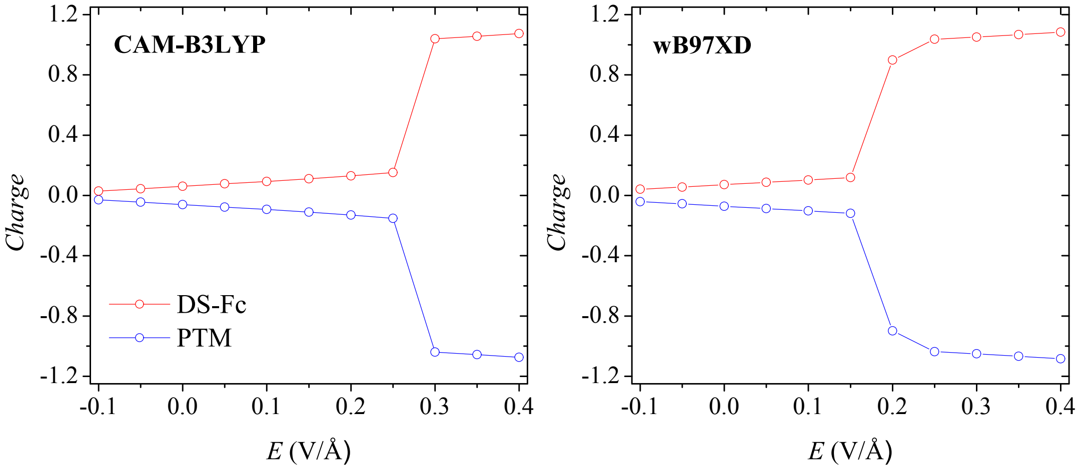

Fig. S8. Calculated Mulliken charges[9] for the DS-Fc (red) and PTM (blue) units as a function of the electric field *E* applied in the direction of the axis formed by the Fe atom and the central C atom of the PTM unit. The long-range correlated hybrid functionals used were CAM-B3LYP [10] (left) and wB97XD[11] (right).

Table S1. Normal component of the dipole (μ_z) and polarizability (α_{zz}) for the isolated molecule **S2**, effective dielectric constants (ε_{eff}) and work-function modification ($\Delta\phi$) in the ground neutral (D-A) and excited zwitterionic states ($(D^+-A^-)'$), as calculated with the (U)wB97XD functional.[11]

State	D-A	$(D^+-A^-)'$
μ_z (D)	-0.35	-11.59
$\alpha_{zz} * 10^{-24}$ (cm^3)	102.64	119.52
ε_{eff}	1.78	1.91
$\Delta\phi$ (eV)	0.07	2.06

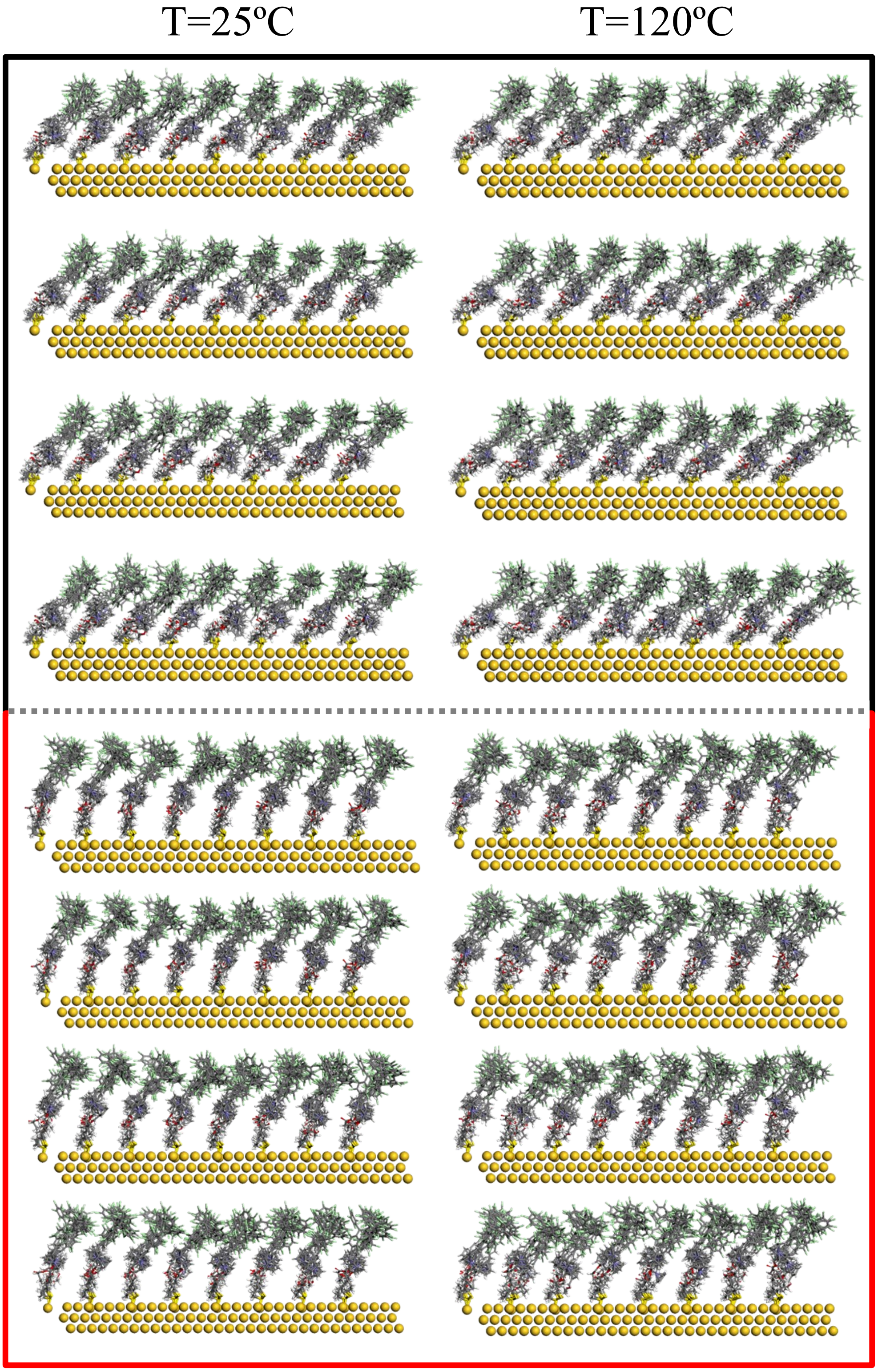

Fig. S9. Lateral view of the unit cell employed in the MM/MD quenched simulations for **S1** (top) **S2** (bottom) with temperatures T=25ºC (left) and T=120ºC (right). The snapshots were taken at simulation times of *t*= 25, 50, 75 and 100 ps from top to bottom.

Note that in the case of **S1** the SAM geometries for both temperatures (25ºC and120ºC) are similar, while **S2** present a considerable increase in the disorder when moving to high temperatures (120 ºC) which can be specially seen for the snapshots at 75 ps and 100 ps.

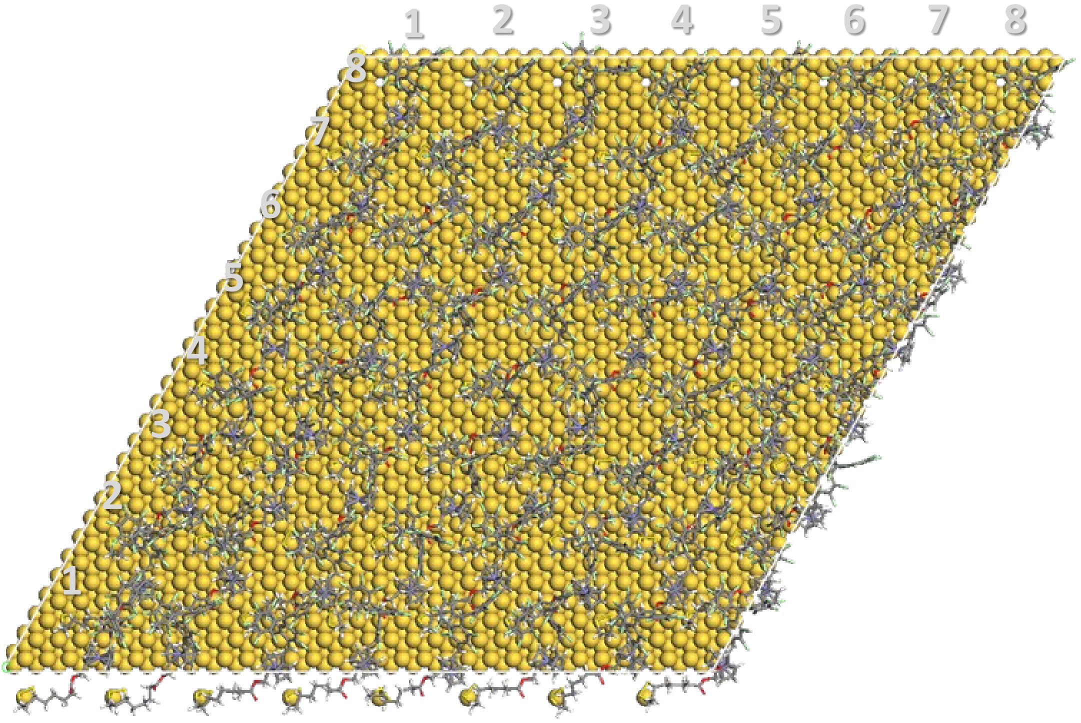

Fig. S10. Top view of the SAM unit cell in the last quenched run performed with **S1** at T=25ºC. The numbers are set over the PTM units and have been used to highlight the 8 rows and the 8 columns of molecules that made the SAM super cell.

7. Author contributions

V.D.-C. and A.G. contributed equally to this work. V. D.-C., M.S., N. G.-P. and A.G. conceived the KPFM experiments and designed the study under the supervision of I.R. and J.V. SAMs were prepared by V. D.-C, N. G.-P. and M.S. KPFM measurements were recorded by V. D.-C., N. G.-P. and A.G. Post-processing analysis of the KPFM measurements was done by A.G. and V. D.-C. Quantum-chemical modelling and Molecular Dynamics simulations were designed and performed by V. D.-C. under the supervision of J.C. The original manuscript has been written by V. D.-C. with contributions from A.G and revisions from J.C, I.R and J.V. All authors contributed to editing of the manuscript and have given approval to the final version. I.R. and J.V. developed the concept of the research.

8. References

[S1] M. Souto, L. Yuan, D. C. Morales, L. Jiang, I. Ratera, C. A. Nijhuis and J. Veciana, *J. Am. Chem. Soc.*, 2017, **139**, 4262−4265.

[S2] M. Gobbi, S. Bonacchi, J. X. Lian, Y. Liu, X.-Y. Wang, M.-A. Stoeckel, M. A. Squillaci, G. D'Avino, A. Narita, K. Müllen, X. Feng, Y. Olivier, D. Beljonne, P. Samorì and E. Orgiu, *Nat. Comm.*, 2017, **8**, 14767.

[S3] B. H. Besler, K. M. Merz Jr. and P. A. Kollman, *J. Comput. Chem.*, 1990, **11**, 431–439.

[S4] M. J. Frisch, M. Head-Gordon and J. A. Pople, *Chem. Phys. Lett.,* 1990, **166**, 275-280**.**

[S5] M. J. Frisch, G. W. Trucks, H. B. Schlegel, G. E. Scuseria, M. A. Robb, J. R. Cheeseman, G. Scalmani, V. Barone, B. Mennucci, G. A. Petersson, H. Nakatsuji, M. Caricato, X. Li, H. P. Hratchian, A. F. Izmaylov, J. Bloino, G. Zheng, J. L. Sonnenberg, M. Hada, M. Ehara, K. Toyota, R. Fukuda, J. Hasegawa, M. Ishida, T. Nakajima, Y. Honda, O. Kitao, H. Nakai, T. Vreven, J. A. Montgomery, Jr., J. E. Peralta, F. Ogliaro, M.

Bearpark, J. J. Heyd, E. Brothers, K. N. Kudin, V. N. Staroverov, R. Kobayashi, J. Normand, K. Raghavachari, A. Rendell, J. C. Burant, S. S. Iyengar, J. Tomasi, M. Cossi, N. Rega, J. M. Millam, M. Klene, J. E. Knox, J. B. Cross, V. Bakken, C. Adamo, J. Jaramillo, R. Gomperts, R. E. Stratmann, O. Yazyev, A. J. Austin, R. Cammi, C. Pomelli, J. W. Ochterski, R. L. Martin, K. Morokuma, V. G. Zakrzewski, G. A. Voth, P. Salvador, J. J. Dannenberg, S. Dapprich, A. D. Daniels, Ö. Farkas, J. B. Foresman, J. V. Ortiz, J. Cioslowski and D. J. Fox, *Gaussian 09, Revision D.01*; 2013, Gaussian Inc. Wallingford, CT, USA.

[S6] W. J. Lauderdale, J. F. Stanton, J. Gauss, J. D. Watts and R. J. Bartlett, *Chem. Phys. Lett.* 1991, **187**, 21-28.

[S7] A. K. Rappe, C. J. Casewit, K. S. Colwell, W. A. Goddard III and W. M. Skiff, *J. Am. Chem. Soc.*, 1992, **114**, 10024–10035.

[S8] *MS Modeling, v7.0.0.0.* 2015, Accelrys Software Inc: San Diego, CA.

[S9] R.S. Mulliken, *J. Am. Chem. Soc.*, 1952, **74**, 811–824.

[S10] T. Yanai , D. P. Tew and N. C. Handy, *Chem. Phys. Lett.*, 2004, **393**, 51–57.

[S11] J.-D. Chai and M. Head-Gordon, *Phys. Chem. Chem. Phys.*, 2008*,* **10**, 6615–6620.